Astronomical and Astrophysical Transactions (*AApTr*), 2025, Vol. 35, Issue 4, pp. 423–430,
ISSN 1055-6796, Photocopying permitted by license only, ©Cambridge Scientific Publishers

The influence of steady temperature on the noise-induced structures in the Orion Bar PDR

I.A. Pomelnikov[1,2,*], D.S. Riashchikov[1,2], D.I. Zavershinskii[2,1], N.E. Molevich[1,2]

[1] *Department of Theoretical Physics, Samara Branch of the Lebedev Physical Institute, 221 Novo-Sadovaya Str., Samara, 443011 Russia*
[2] *Department of Physics, Samara National Research University, 34 Moskovskoye Shosse, Samara, 443086 Russia*

Received 15 June, 2025; accepted 30 August, 2025

We present the results of numerical modelling of noise-induced structures evolution in the atomic zone of the Orion Bar photodissociation region (PDR). We conducted numerical experiments with the isentropically unstable medium with initial disturbances in a form of noise signal. The modelling results showed satisfactory agreement between the characteristic sizes of structures formed from a noise signal and structures formed from a Gaussian disturbance. In addition, the sizes of the obtained structures match the widths of the dense periodic structures observed in the Orion Bar.

Keywords: Instabilities – shock waves – ISM: clouds – ISM: photon-dominated region (PDR) – ISM: individual objects: Orion Bar

1 Introduction

One of the most studied photodissociation regions (PDRs) is the Orion Bar, located in the Orion Nebula near the Trapezium cluster. In the atomic zone of the Orion Bar, small-scale inclusions of dense gas are observed within a less dense medium (Goicoechea et al., 2016). Recent studies using JWST (Habart et al., 2024) and Keck (Habart et al., 2023) telescopes have revealed thin extended structures near the dissociation front with widths of $(1\text{–}20)\times10^{-3}$ pc, spaced approximately 2×10^{-2} pc apart, exhibiting sharp density gradients.

Observations of Bron et al. (2018), Joblin et al. (2019), Kavak et al. (2022), Habart et al. (2023), and Habart et al. (2024) indicate non-thermal gas motions in the Orion Bar PDR. The turbulent velocity in dense structures reaches about 0.49 of the sound speed (Ferland et al., 2012). These dense regions also show elevated pressure and temperature compared to the surrounding gas (Goicoechea et al., 2016). Similar thin structures with anomalous turbulent velocities have been detected in other PDRs:

*Email: pomelnikovia@smr.lebedev.ru

S187 (Zemlyanukha et al., 2022) and the Carina's Westrn Wall PDR (Hartigan et al., 2020, Downes et al., 2022), though none as detailed as in Orion Bar due to greater distances.

Heating and cooling processes in the medium can be described as a generalized heat-loss function dependent on hydrogen concentration and temperature:

$$\mathfrak{J}(n,T) = \Lambda(n,T) - \Gamma(n,T), \tag{1}$$

where $\Lambda(n,T)$ is the cooling rate, and $\Gamma(n,T)$ is the heating rate of the medium, n is the atomic hydrogen number density, and T is the temperature of the medium. The conditions involving derivatives of this function determine the type of instability according to Field's classification (Field, 1965). There are isochoric, isobaric and isentropic instabilities.

The isochoric instability leads to exponential temperature growth, which remains spatially uniform throughout the unstable region. This avoids the formation of distinct structures, but pressure variations accompanying the isochoric temperature changes will generally drive motions that destroy the constant density. Therefore, this criterion is not consistent with the description of dynamic structures.

Within the isobaric instability, the initial perturbations develop extremely rapidly. This leads to the formation of a pronounced contrast between regions: cold, very dense clumps emerge, surrounded by a hot and extremely rarefied medium. This strong density imbalance, which exists under conditions of pressure equilibrium, creates ideal conditions for the onset of matter condensation, during which the mass of the dense clump can significantly increase through the accretion of surrounding material.

Finally, isentropic (acoustic) instability leads to additional heat release in the areas of acoustic wave compression. This positive feedback between acoustic disturbances and heating leads to an amplification of the acoustic wave. Acoustic instability leads to the formation of areas of density, temperature, and pressure growth. The propagation of a hydrodynamic disturbance in an isentropically unstable medium can result in its transformation into a sequence of autowave pulses (Molevich, 2011, Krasnobaev & Tagirova, 2017, Molevich & Riashchikov, 2021, and Riashchikov et al., 2022).

In modern theoretical works related to the Orion Bar study, stationary isobaric and isochoric models are used to analyze the chemical composition of the medium (Goicoechea et al., 2016, Joblin et al., 2018, Habart et al., 2024). Despite the fact that these models accurately predict the distribution of chemicals in the PDR, the models basically do not involve a study of the observed turbulent velocity in the medium. At the same time, as shown by Krasnobaev & Tagirova (2017) and Molevich & Riashchikov (2021), the Orion Bar satisfies the conditions for isentropic instability. This enables us to interpret the processes in its PDR as gas-dynamic disturbances that, at late evolutionary stages, may evolve into self-sustaining shockwave structures (autowave pulses).

In (Pomelnikov, 2025), we examined the formation of such structures in the Orion Bar PDR triggered by initial localized perturbations. In the present paper, we investigate their evolution under the same conditions but with disturbances of small width and amplitude, that are present throughout the entire volume. This initial condition we call noise signal.

2 Model

We analyse dynamic structures in isentropically unstable media using hydrodynamic equations system:

$$\frac{\partial \rho}{\partial t} + \frac{\partial}{\partial z}(\rho v) = 0, \tag{2}$$

$$\rho\left(\frac{dv}{dt} + v\frac{\partial v}{\partial z}\right) = -\frac{\partial P}{\partial z}, \tag{3}$$

$$C_{V\infty}\frac{dT}{dt} - \frac{k_B T}{m\rho}\frac{d\rho}{dt} = -\mathfrak{J}(n,T), \tag{4}$$

$$P = \frac{k_B \rho T}{m}. \tag{5}$$

Here, Eq. (2) is the equation of continuity, Eq. (3) is the equation of motion, Eq. (4) is the heat transfer equation, where $C_{V\infty}$ is the heat capacity at constant volume, k_B is the Boltzmann constant, m is the mass of the hydrogen atom, $\mathfrak{J}(n,T)$ is the heat loss function (1), Eq. (5) is the equation of state. The derivative $d/dt = \partial/\partial t + v\ \partial/\partial z$ is a substantial derivative. In the system of Eqs. (2)–(5), $\rho = nm,\ P,\ v,\ T$ are density, pressure, gas dynamic velocity and temperature, respectively.

Krasnobaev et al. (2017) presented function (1) in the following form:

$$\mathfrak{J}(n,T) = (\Lambda_{CII158} + \Lambda_{OI63} + \Lambda_{OI146}) + \Lambda_{pe} - \Gamma_{pe}. \tag{6}$$

Here, Γ_{pe} is heating due to the photoelectron effect on polycyclic aromatic hydrocarbon (PAH) molecules and small dust particles; Λ_{pe} is cooling due to energy loss during accretion of charged particles on the dust surface; Λ_{CII158}, Λ_{OI63}, Λ_{OI146} are cooling caused by the emission of spectral lines [CII] 158 μm, [OI] 63 μm, and [OI] 146 μm.

In the following calculations, we employ the possible values of the parameters that influence the equilibrium of heating and cooling in the Orion Bar PDR, which are presented in Table 1. G_0 is the light field around the medium. $t_C,\ R_V,\ b_C$ are the values of light absorption and scattering by the medium. $\xi_C,\ \xi_O$ are abundances of carbon and oxygen to the concentration of hydrogen.

We consider stationary temperature T_0 range as 500–2000 K. According to (Bron et al., 2018, Joblin et al., 2019, Kavak et al., 2022), these temperature values are shown in the descriptions of the Orion Bar atomic region observations, and according to (Pomelnikov et al., 2025), the condition of isentropic instability is fulfilled at temperatures $T_0 \gtrsim 500$ K. Using the equation $\mathfrak{J}(n_0, T_0) = 0$ for medium steady state, we can obtain the $n_0(T_0)$ dependency and find the values of number density for the range of specified temperatures. As it can be seen in Fig. 1, the values of n_0 are in the range of $(1.0 - 4.0) \times 10^5$ cm^{-3}. These values correlate with the values of number density described by Joblin et al. (2019), Habart et al. (2023), and Habart et al. (2024).

Table 1 Numerical parameters for Orion Bar PDR modelling.

Parameter	Value	Refs.
G_0 (Habing units)	4.0×10^{4}	1–5
τ_C	0.5	6, 7
ξ_C	1.2×10^{-4}	7
ξ_O	2.56×10^{-4}	7
R_V	5.5	8
b_C	3.0×10^{-5}	8

* References: 1. Joblin et al. (2018); 2. Goicoechea et al. (2016); 3. Salgado et al. (2016); 4. Habart et al. (2023); 5. Habart et al. (2024); 6. Tielens (2005); 7. Krasnobaev & Tagirova (2017); 8. Wakelam et al. (2008).

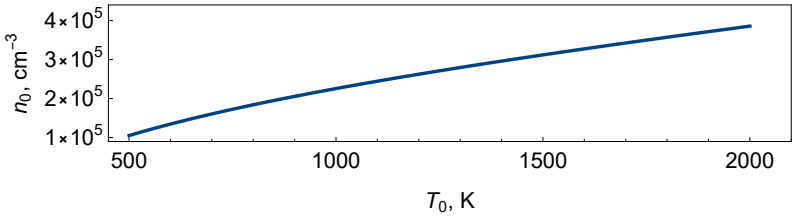


Figure 1 The ratio between number density n_0 and temperature T_0 in the steady state of the medium with parameters of the Orion Bar PDR.

3 Evolution of noise-induced structures

To study the evolution of noise-induced structures, we define the initial perturbation of the medium in each node of the computational grid as follows:

$$\rho = (1+\epsilon)\rho_0, \quad P = (1+\epsilon)P_0, \tag{7}$$

where ϵ is a random variable distributed in the interval $[-\delta, \delta]$, $\delta = 0.01$.

To study the behaviour of noise-induced structures in an atomic gas cloud, we use a system of Eqs. (2)–(5). We conduct our numerical experiments through the Athena++ code (Stone, 2020), using the LHLLC Riemann solver. For the medium simulation, in this work, we use periodic boundary conditions.

The numerical scheme, which incorporates the established heat-loss function, was validated and its grid parameters were optimized through comparison with exact analytical shockwave solutions (Molevich & Riashchikov, 2021). A comprehensive description of this validation and parameter selection process is provided in the Appendix of Pomelnikov et al. (2025).

The dependence of the total energy growth in the modelled system over time is demonstrated in Fig. 2. This figure shows that up to that time $\tau \approx 50,000$ years, the total energy of the system, and hence, the amplitudes of individual pulses grow regardless of their collisions with each other. After overcoming this time point, the value of the total energy of the simulated system reaches its maximum value and the development of individual pulses as autowave structures stops. This limitation of the

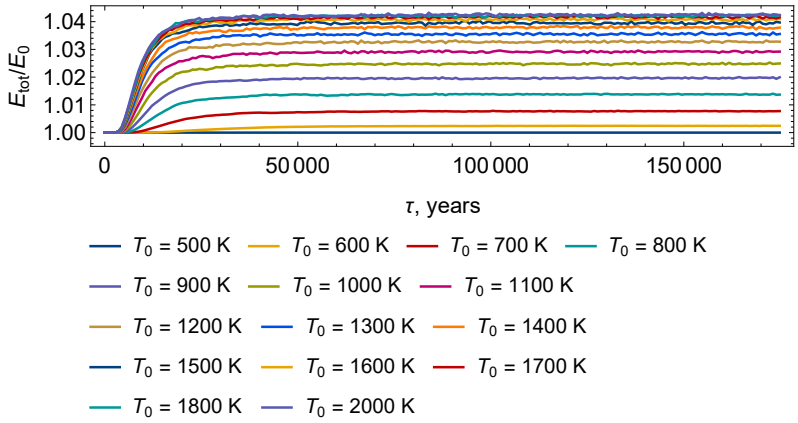


Figure 2 Evolution of the system total energy for different stationary temperature values during the evolution of dynamic structures from noise signal. E_0 denotes the total energy of the unperturbed medium.

energy growth of the medium correlates with the limitation of the amplitude growth during the evolution of structures from a localized disturbance (Pomelnikov et al., 2025).

We now direct our attention to the morphology of the structures that emerge from the initial noise signal once the total energy of the medium has saturated, as illustrated in Fig. 3.

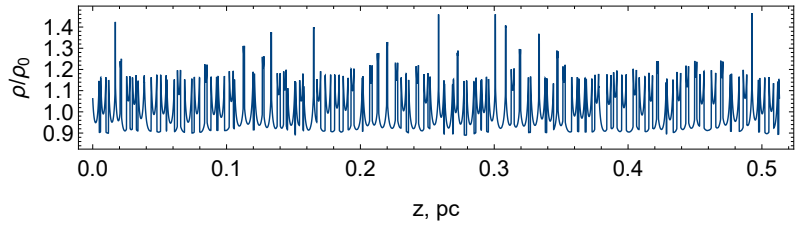


Figure 3 Structures formed from noise in an isentropically unstable medium at $T_0 = 1000\,\mathrm{K}$. The density distribution corresponds to the time point $\tau \approx 174,000$ years.

Note that the spatio-temporal structure formed in Fig. 3 consists of a series of shock waves travelling in the positive and negative directions of the z-axis.

4 Discussion

The morphology of the spatial structure demonstrated in Fig. 3 reveals a series of shock wave pulses propagating in various directions. While the given structure lacks a pronounced period, however, through the Fourier transform, a characteristic scale, determined by the heating and cooling processes, and thus by the parameters of the steady state, can be deduced through Fourier analysis. Although Fourier analysis

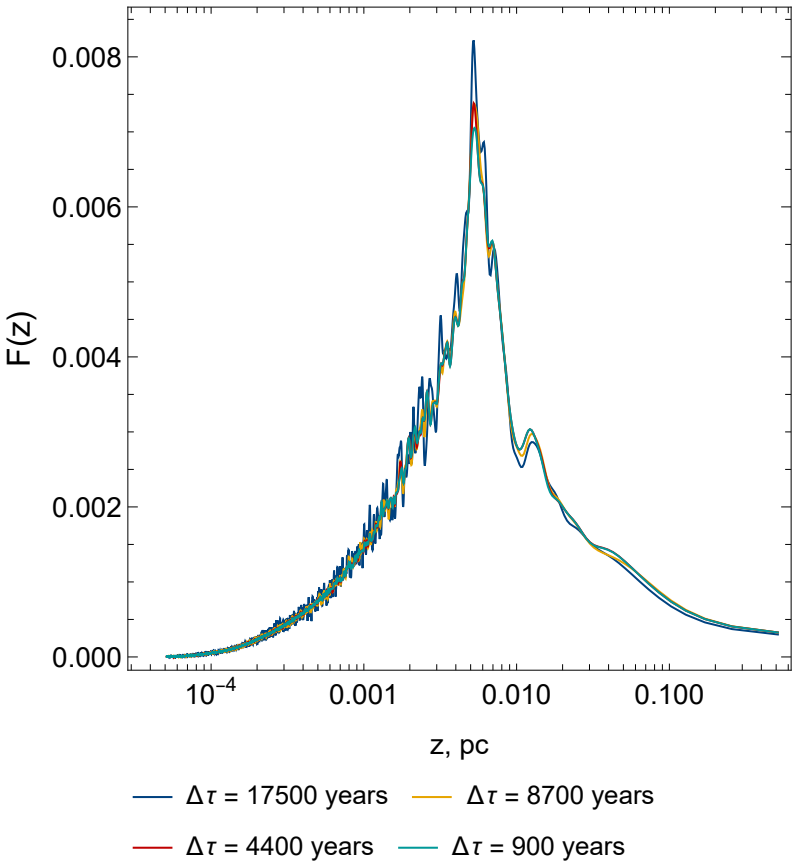


Figure 4 The average spectrum of noise-induced structures for the case $T_0 = 1000\,\mathrm{K}$ at time points from 50,000 to 170,000 years with different averaging intervals $\Delta\tau$.

reveals the presence of a maximum, whose position on the coordinate axis is considered to be the characteristic size, in a particular wavelength range, its position may shift slightly in different orientations at different points in time during the simulation, due to the stochastic nature of the initial perturbation, and consequently, the stochastic nature of the density distribution at any given instant in time. In order to minimize the potential for errors in determining the characteristic size of simulated structures, we compute the average Fourier spectrum derived from the Fourier transforms of spatial density distributions at various time points after the development of the structure has concluded, i.e., at points where the total energy of the system has reached its maximum value. This averaging is performed across time points beginning at $\tau = 50,000$ years with different time step increments (averaging intervals) along the time grid. Figure 4 illustrates the averaging of the same distribution for various averaging intervals $\Delta\tau$ ranging from 17,500 to 900 years.

According to Fig. 4, the characteristic size is approximately 10^{-2} pc at each averaging interval with the stationary temperature $T_0 = 1000$ K. In addition to this, we have investigated the dependence of the characteristic scale of structures on the

stationary temperature T_0. In Fig. 5 we see that the value of this characteristic scale is about 5.0×10^{-3} pc at 600 K and does not undergo significant changes with T_0 increasing.

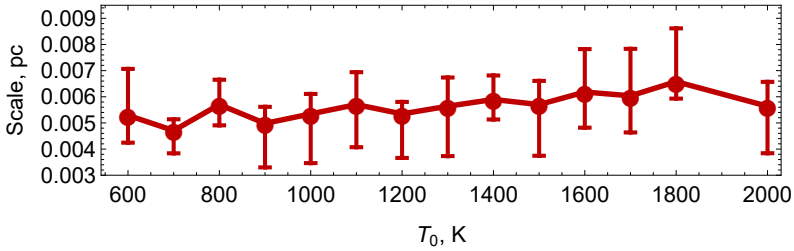


Figure 5 The characteristic size of the structures formed from the noise signal depending on the stationary temperature T_0.

It is important that structures emerging from noise signals in isentropically unstable regions exhibit finite amplitudes and a characteristic period of $\gtrsim 5.0 \times 10^{-3}$ pc. Comparison with the previously obtained results for the characteristic sizes shows a good agreement with both the sizes of dense structures observed in the Orion Bar PDR (Habart et al., 2023, Habart et al., 2024) and the widths of shock wave pulses obtained using numerical and analytical calculations given in Pomelnikov et al. (2025). This result demonstrates the common nature of shockwave structures developing from different initial perturbations.

Acknowledgements

This work was supported in part by the Ministry of Science and Higher Education of the Russian Federation under State assignment to educational and research institutions under Project No. FSSS-2023-0009 and FFMR-2024-0017. We also acknowledge the use of data from ALMA, Herschel, Keck, and JWST, which have been instrumental in advancing our understanding of the Orion Bar PDR.

References

Bron E. et al. (2018) arXiv preprint arXiv:1801.01547.
Downes T. P. et al. (2023) MNRAS, 519(4), 5427-5438.
Ferland G. J. et al. (2012) ApJ, 757(1), 79.
Field G. B. (1965) ApJ, 142, 531–567.
Goicoechea J. R. et al. (2016) Nature, 537(7619), 207-209.
Habart E. et al. (2023) A&A, 673, A149.
Habart E. et al. (2024) A&A, 685, A73.
Hartigan P. (2022) ApJ, 164(6), 257.
Joblin C. et al. (2018) A&A, 615, A129.
Kavak U. et al. (2022) A&A, 660, A109.

Krasnobaev K. V., Tagirova R. R. (2017) MNRAS, 469, 1403–1413.
Molevich N. et al. (2011) Astrophys. and Space Sci., 334, 35.
Molevich N., Riashchikov D. (2021) Physics of Fluids, 33(7), 076110.
Pomelnikov I. A. et al. (2025) A&A, DOI: 10.1051/0004-6361/202554479.
Riashchikov D. S., Pomelnikov I. A., Molevich N. E. (2022) Bulletin of the Lebedev Physics Institute, 49, 307.
Stone J. M. et al. (2020) ApJ Supp. Ser., 249, 4.
Zemlyanukha P. et al. (2022) MNRAS, 515(2), 2445-2463.